Electron Microscopy and MR Imaging Findings in Embolic Effects

Byung-Rae Park[1†] and Bong-Oh Koo[2]

[1]Department of Radiological Science, [2]Department of Physical Theraphy,
Catholic University of Pusan, Busan 609-757, Korea

Evaluated the hyperacute embolic effects of triolein and oleic acid in cat brains by using MR image and electron microscopy. In fat embolism, free fatty acid is more toxic than neutral fat in terms of tissue damage. T2-Weighted imaging, diffusion-weighted imaging, and contrast-enhanced T1-weighted imaging were performed in cat brains after the injection of triolein (group 1, n=8) or oleic acid (group 2, n=10) into the internal carotid artery. MR image were quantitatively assessed by comparing the lesions with their counterparts on T2-weighted images, apparent diffusion coefficient (ADC) maps, and contrast-enhanced T1-weighted images. Electron microscopic findings in group 1 were compared with those in group 2. Qualitatively, MR images revealed two types of lesions. Type 1 lesions were hyperintense on diffusion-weighted images and hypointense of ADC maps. Type 2 lesions were isointense or mildly hyperintense on diffusion-weighted images and isointense on ADC maps. Quantitatively, the signal intensity rations of type 1 lesions in group 2 specimens were significantly higher on T2-weighted images $(P=.013)/(P=.027)$ and lower on ADC maps compared with those of group 1. Electron microscopy of type 1 lesions in both groups revealed more prominent widening of the perivascular space and swelling of the neural cells in groups 1. MR and electron microscopic data on cerebral fat embolism induced by either triolein or oleic acid revealed characteristics suggestive of both vasogenic and cytotoxic edema in the hyperacute stage. Tissue damage appeared more severe in the oleic acid group than in the triolein group.

Key Words: Electron microscopy, Fat embolism, Apparent diffusion coefficient maps

INTRODUCTION

The classic mechanism of fat embolism syndrome is explained by mechanical and biochemical theories. Experimental animal models of fat embolism generally focus on lung injury, because the lung is the primary site of fat embolism in patients with trauma. However, because neurologic signs can precede respiratory symptoms, the brain may reveal more distinctive pathologic characteristics. The mechanical theory postulates that triglyceride particles from injured adipose tissue enter the circulation and obstruct the pulmonary vessels. The biochemical hypothesis implicates free fatty acids, proposing that local hydrolysis of trigly-

ceride emboli by pneumocyte lipase, together with excessive mobilization of free fatty acids from peripheral adipose tissue by stress hormones, results in the toxic concentration of these acids in the lungs (Nakata et al., 1999).

Experimental reports of cerebral fat embolism are rate. The blood-brain barrier is disrupted within 30 minutes after neutral fat embolization Hyperintensity on T2-weighted images and lesional enhancement on contrast-enhanced T1-weighted images are related to defects in the endothelial wall and the early appearance of vasogenic edema. However, in the brain, the blood-brain barrier opens within 15 minutes (Drew et al., 1988), after its exposure to triolein. Delivery of molecules from the blood into the central nervous system is limited and depends on lipidsolubility and the molecular mass and charge (Kroll et al., 1988). Conparisons of the histopathologic findings (Jones et al., 1982), reveal that free fatty acids are more toxic than neutral fat in the lung and kidney. Kim et al (Kim et al., 2001), studied only the effect of neutral fat, and to our knowledge, the different fat emboli in the brain have not been compared.

The present study was conducted to evaluate the differences in embolic effects between two groups: those embolized with triolein (neutral fat) and those embolized with oleic acid (free fatty acid). We used MR imaging and electron microscopy to compare the embolic effects in the two groups.

MATERIALS AND METHODS

1. Experimental Design of Animal Models

Cats were anesthetized with intramuscular injection of ketamine HCL (2.5 mg/kg; Korea United Pharm Inc., Seoul Korea) and xylazine (0.125 mg/kg; Bayer Korea, Seoul, Korea). Body temperatures were measured by using a rectal probe (MGA-III 219; Shnbaura Electronics Co. Ltd., Tokyo, Japan) and maintained at 37~37.5℃. We placed an 18-gauge angiographic catheters (Angiocath; Becton Dickinson, UT) in the left femoral artery for the injection of a contrast material or drugs to allow monitoring of the blood pressure and blood gas levels in the left femoral vein. The right femoral artery was isolated, and another 18-gauge angiographic catheter (Angiocath; Becton Dickinson) was inserted into the artery. A 3F microcatheter (MicroFerret-18 infusion catheter; William Cook Europe, Bjaeverskov, Denmark) was passed through the angiograpic catheter into the lumen of the artery. The right internal carotid artery was selected. The tip of the microcatheter was positioned just proximal to the entrance of the intracranial portion of the internal carotid artery.

The acts were assigned to one of two groups: Group 1 (n=8) received a single 0.1 ml dose of neutral triglyceride triolein (1,2,3-tri [cis-9-octadecenoyl] glycerol, Sigma, St Louis, MO) and group 2 (n=10) were treated with 0.1 ml of oleic acid (cis-0-octadecenoic acid; Sigma), by using a 1 ml syringe. After the treatment with triolein or oleic acid, 2 ml of saline was injected with a 2 ml syringe over 30 seconds.

2. Magnetic Resonance Imaging

Cats were placed in a prone position in a pediatric MR positioning device, and a small field of view (FOV) radio-frequency coil (Siemens, Erlangen, Germany) was placed above its head. All studies were performed with a 1.5-T MR unit (Vision; Siemens). Serial MR imagind was performed at 30 minutes and 2 hours after embolization. Images were acquired in the coronal plane. For spin-echo imaging,

the following parameters were used: TR/TE/NEX of 3000/96/2 for T2-weighted sequences and 320/20/2 for T1-weighted sequences, a section thickness of 4 mm with a 0.1 mm gap, an FOV of 70~75 mm, and an acquisition matrix of 210×256. Diffusion-weighted imaging was performed using an echo-planar sequence. The imaging parameters were as follows: an FOV of 130 mm, 128 phase-encoding steps, a section thickness of 4 mm, a gap of 0.1 mm, and an acquisition matrix of 96×160. The diffusion sensitizing gradient was oriented at the y-axis (ventral to dorsal) with b values of 0 and 1000 s/mm^2. The apparent diffusion coefficient (ADC) map was obtained by using custom software (Pusan National University Hospital, Pusan, Korea). For contrast-enhanced studies, 0.2 mM/kg gadopentetate dimeglumine (Magnevist; Schering, Germany) was injected intravenously.

3. MR Images Analysis

Qualitative Assessments; Diffusion-weighted image, T2-weighted images, ADC maps, and contrast-enhanced T1-weighted images obtained in the two groups were analyzed for the presence and area of abnormal signal intensity. High signal intensity on T2-weighted images or diffusion-weighted imaged or low signal intensity on the ADC maps or enhancement on contrast-enhanced T1-weighted images, at either examination was defined as a lesion.

Quantitative Analyses; Signal intensity ratios on T2-weighted images, ADC maps, and contrast-enhanced T1-weighted images were measured in both groups. The signal intensity ratio of interest of an obviously abnormal lesion to that of the normal areas were counted. On serial images obtained in the same cat, the size and position of the region of interest of an obviously abnormal lesion to that of the normal contralateral hemisphere. If the counterpart were affected, adjacent normal areas were counted.

On serial images obtained in the same cat. the size and position of region of interest were identical. The significance of the differences in the signal intensity ratio between group 1 and group 2 and the changes in the signal intensity ratio over time were estimated in an analysis of variance based on repeated measurements.

4. Electron Microscopy

Immediately after the cats were sacrificed by using sodium thiopental their brains were excised, and a homemade

cutting device was used to dissect them into 4 mm thick sections in the same coronal plane as that of the MR images. Three areas of gray matter that correlation to lesions observed on the MR images were selected. these areas were cut into 1 mm³ cubes to prepare blocks for electron microscopy. Samples were prefixed with 2.5% glutaraldehyde in phosphate-buffered saline at pH 7.2 for 2 hours at 1~4℃ and washed in 0.1 mol/L phosphate-buffered saline. Next, samples were fixed in 1% OsO₄ solution for 2 hours and washed in the same solution. After washing, the samples were dehydrated with alcohol, treated in a mordant en bloc overnight with Polybed 812 resin (Poly-sciences, Warrington, PA) and stored for 12 hours at 37℃ and then for 48 hours at 45℃. The resin-embedded blocks were cut into 1 μm thick sections and stained with toluidine blue. Areas of interest were then selected under a light microscopy. Ultra-thin sections were prepared by suing an ultramicrotome (Leica, Vein, Austria) with a diamond knife and applied to nickel 150 mesh grids. Samples were stained with uranyl acetate and lead citrate and examined with a transmission electron microscope (JEM 1200 EX-II; JEOL Tokyo, Japan).

The presence of capillary endothelial wall, widening of the perivascular interstitial space, and neural cellular swelling were evaluated. The mean number of intravascular fat vacuoles was calculated within five mesh spaces in the field. Perivascular interstitial space winening was classified as mild or servere. Mild widening was classified as mild if the diameter of a swollen cell was less than 5 μm or severe if the diameter was greater than 5 μm.

RESULTS

1. Qualitative Assessment with MRI

Both types were simultaneously present in seven cats. Type 1 lesions were commonly observed in the medical portion of the superficial gray matter and white matter of the hemishpere, whereas type 2 lesions frequently surrounded the type 1 lesions and were larger. One cat of group 1had only type 2 lesions; no definite type 1 lesion could be identified in this particular cat. In all eight cats, lesions were located in the ipsilateral superficial gray matter, most commonly at the medical and posterior portions of the hemisphere. The ipsilateral white matter was affected in six cats. In five cats, the ipsilateral deep gray matter was additionally involved. Contralateral superficial gray matter was focally
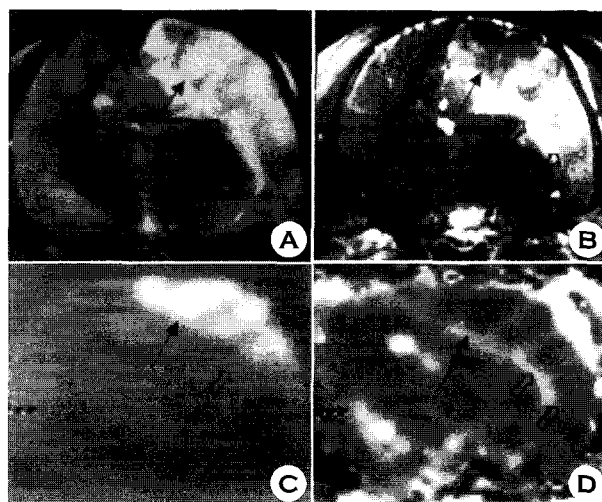

Fig. 1. Group 2. MR images obtained 2 hours after cat brains were embolized with oleic acid group show type 1 (solid arrow) and type 2 (open arrows)lesions.
A, T2-weighted (3000/96/2) image. Type 1 lesions have mild hyperintensity. Type 2 lesions are hyperintense. B, Contrast-enhaced T1-weighted (320/30/2) image. Type 1 lesions show less enhancement than do type 2 lesions, which show strong enhancement. C, Diffision-weighted image. Type 1 lesions are hyperintense. Type 2 lesions have isointensity or mild hyperintensity. D, ADC map. Type 1 lesions are hypointense. Type 2 lesions are isointense.

affected in four cats.

In the 10 animals in group 2, two types of lesions were present, similar to those of group 1 (Fig. 1). Both types were simultaneously present in eight cats, whereas only type 2 lesions were observed in two animals. The ipsilateral superficial gray matter was affected in all cats, and ioslateral white matter was affected in nine cats. Contralateral superficial gray matter was affected in two cats. Ipsilateral deep gry matter was affected in seven cats, and the brain stem was affected in six cats. T2-weighted images, diffusion-weighted images, and ADC maps generally showed more prominent abnormal signal intensity in the group 2 animals, compared with those of group 1. However, contrast enhancement on contrast-enhanced T1-weighted images was less prominent in group 2.

Lesions in both groups were more prominent in images obtained at 2 hours, compared with those obtained at 30 minutes. Lesions did not change in type over the measured time period in all cats in both groups. However, the size of lesions was slightly increased at 2 hours, compared with their size at 30 minutes, and they extended to the white matter in some cats.

Table 1. Mean signal intensity ratios of the lesions on T2-weighted images

Group and Lesion	Signal Intensity Ratio	
	At 30 min	At 2 h
1, triolein (n=8)		
Type 1 (n=7)	1.14 (0.08)*	1.41 (0.08)*
Type 2 (n=8)	1.21 (0.15)	1.36 (0.09)
2, oleic acid (n=10)		
Type 1 (n=8)	1.23 (0.10)*	1.67 (0.24)*
Type 2 (n=10)	1.15 (0.14)	1.36 (0.17)

The data are the mean ± SD
*In type 1 lesion, the signal intensity ratios were significantly higher in group 2 compared with group 1 at both 30 minutes and 2 hours ($P<.013$). However, in type 2 lesions, the signal intensity ratios did not significantly differ between the two groups at either time point ($P>.643$)

Table 2. Mean signal intensity ratios of the lesions on ADC maps

Group and Lesion	Signal Intensity Ratio	
	At 30 min	At 2 h
1, triolein (n=8)		
Type 1 (n=7)	0.72 (0.12)	0.67 (0.12)
Type 2 (n=8)	0.97 (0.16)	1.12 (0.28)
2, oleic acid (n=10)		
Type 1 (n=8)	0.61 (0.08)	0.60 (0.11)
Type 2 (n=10)	0.91 (0.18)	0.95 (0.13)

The data are the mean ± SD
*In type 1 lesion, the signal intensity ratios were significantly lower in group 2 compared with those in group 1 at both 30 minutes and 2 hours ($P=.027$). However, in type 2 lesions, the signal intensity ratios did not significantly differ between the two groups at either time point ($P=.144$)

2. Quantitative Measurements on MR Images

Signal intensity rations of both types of lesions in group 1 and 2 animals were measured. On T2-weighted images (Fig. 2, Table 1), the signal intensity rations of type 1 lesions in group 2 were statistically higher than those in group 1 ($P=.013$). For type 2 lesions, however, signal intensity rations were not significantly different between the groups ($P>.643$). The signal intensity rations of both groups significantly increased at 2 hours compared with those at 30 minutes ($P<.001$). Signal intensity rations in type 1 lesions were significantly higher than those in type 2 lesions in group 2 ($P<.042$).

On the ADC maps (Fig. 3, Table 2), in type 1 lesions, the signal intensity rations were significantly lower in group 2 compared with those in group 1 at both 30 minutes and 2
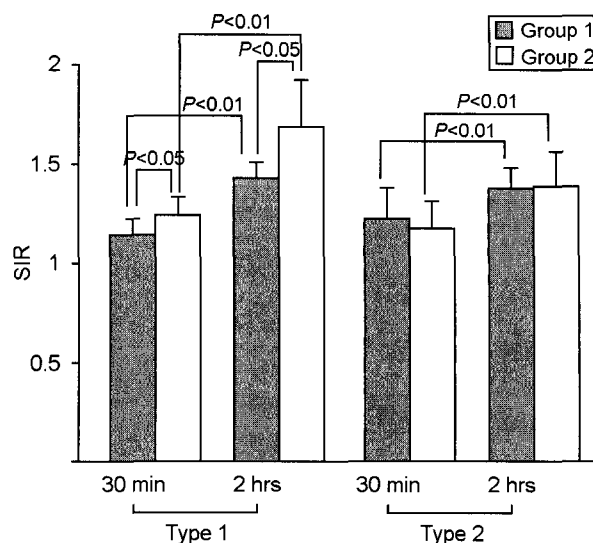

Fig. 2. Bar graph of the signal intensity rations on T2-weighted images. At 2 hours, the rations in type 1 and type 2 lesions increase significantly in both groups ($P<.001$). The rations of type 1 lesions are significantly higher in griup 2 compared with group 1 at both 30 minutes and 2 hours ($P=.013$). However, in type 2 lesions, the rations do not significantly differ in either group at either time ($P>.643$).
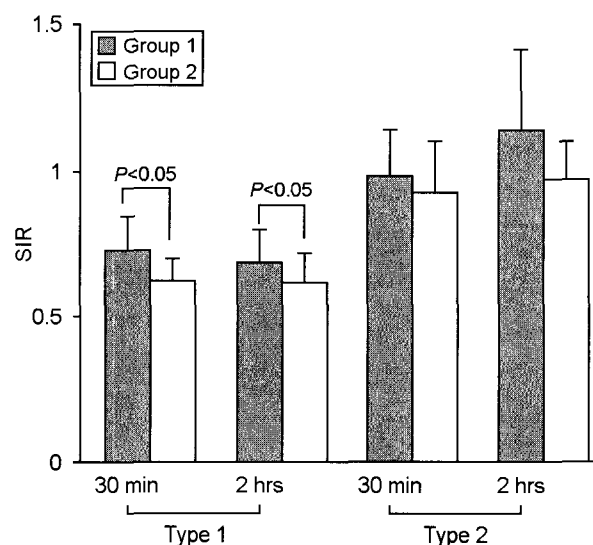

Fig. 3. Bar graph of the signal intensity rations on the ADC maps. Compared with the baseline value at 30 minutes, the rations in types 1 and type 2 lesions did not change sigficantly at 2 hours in either group ($P>.485$). With the type 1 lesions, the rations in group 2 were sigficantly lower than thouse in group 1 at each time point ($P=.027$). However, in type 2 lesions, the rations were not sigficantly different in either group ($P>.144$).

hours ($P=.144$). Notably, signal intensity rations in type 1 lesions were lower than those of type 2 in both groups at each time point ($P<.001$). No significant changes were ob-

Fig. 4. Electron microscopy findings in a type 1 lesion in a cat brain from group 1, which was treated with triolein (original magnification ×3000). Photomicrograph shows an intravascular fat vacuole (F) and defects in the endothelial wall (solid arrows). Areas of perivascular interstitial edema (asterisk) and neuropil swelling (arrowhead) are smaller than 5 μm in diameter. Open arrows represent red blood cells. Bar indicates 2 μm.

Fig. 5. Electron microscopy findings in a type 1 lesion in a cat brain from group 2, which was treated with oleic acid (original magnification ×4000). Neuropil cells (arrowheads) are edematous, and widening of the interstitial spce (asterisk) is prominent. Bar indicates 2 μm.

served in signal intensity rations in the time-course experiments ($P>.485$).

On contrast-enhanced T1-weighted images, the signal intensity rations in type 2 lesions in group 1 were significantly higher than those in group 2 ($P<.001$). In the time-course experiments, a significantly rations in type 1 lesions ($P=.013$) but not in type 2 lesions ($P>.683$). In group 1, signal intensity rations in type 2 lesions were generally higher than those in type 1 lesions ($P=.001$).

3. Electron Microscopy Findings

In group 1 (triolein group), intravascular fat vacuoles and endothelial defects were frequently observed (Fig. 4). Widening of the perivascular interstitial space was mild in seven cats, including one cat with only type 2 lesions. This widening was severe in on cat. Neuropil swelling was mild in six cats, including one cat with only type 2 lesions. This swelling was severe in two cats. In all cats, intravascular fat vacuoles were present within the dilated lumen. The num-

ber of intravascular fatvacules in five mesh spaces ranged from 0.2 to 5. The sizes varied, ranging from 10 to 50 μm. Endothelial cells were stretched thin because of the vacuoles. In larger arterioles, the vacuoles were commonly elongated or sausage-shaped. Fat vacuoles appeared homogeneous, round, and less dark compared with the red blood cells. Defects in the endothelial wall were frequently observed in six cats. Tiny pinocytic vacuoles were sporadically noted on the endothelial walls. Phagocytosed fat vacuoles measuring 0.25~1 μm in diameter were also present in two cats. The enlarged perivascular interstitial spaces contained fluid that frequently included various microstructures such as lysosomes, mitochondria, destroyed cell membranes, or red blood cells, The perivascular fluid was identical to the intravascular plasma.

In group 2 (oleic acid-treated) animals, intra and extravascular fat vacuoles (with diameters as large as 5 and 20 μm, respectively) were prevalent in all cats. Widening of the perivascular interstitial space and cellular swelling was serve in eight cats that had both types of lesions. Two cats

had only type 2lesions. In one cat, widening of the peri-vascular space and celluar swelling were mild; in another, they were serve. The mean number of intravascular fat vacuoles in five mesh spaces was 0.2. Fat vacuoles were coarse, inhomogeneous, and small compared with those of group 1, and they were less dark than red blood cells. No defects but numerous pinocytic fat vacuoles were observed on the endothelial walls, in contrast to the findings in group 1 (Fig. 5).

DISCUSSION

Oleic acid is the most important constituent acid in human fat (Peltier et al., 1956). Unsaturated fatty acids account for 65~80% of the constituent acids. Human fat obtained from the long bones and subcutaneous tissue is almost entirely neutral fat (triglyceride, esters of glycerol, and long chain fatty acids). Free fatty acids are normally produced upon the hydrolysis of triglycerides by lipase in fat deposits. These acids usually bind serum albumin. Consequently, less than 1% of the free fatty acids in the serum exist in the unbound state (Moylan et al., 1976). The general pathophysiology of fat embolism is currently under investigation. To date, tissue damage is believed to be the result of a combination of the mechanical and biochemical effects of fat (Cossling et al., 1982; Peltier, 1969). Findings from a number of studies in-dicate that neutral fat initiates a mechanical block of the arterial circulation when it is introduced intravenously, whe-reas free fatty acids result in delayed extensive biochemical inflammatory tissue destruction on the second or third day after trauma (Reidbord, 1984). The present study revealed two types of MR imaging findings with cerebral fat embo-lism in both groups. The first, type 1, appears as high signal intensity on T2-weighted images and diffusion-weighted images, as low signal intensity on ADC maps, and as mild enhancement on contrast-enhanced T1-weighted images. The other, type 2, has mildly high signal intensity on T2-weighted images and diffusion-weighted images, isointense signal on ADC maps, and enhancement on contrast enhan-ced T1-weighted images. Type 1 resembles findings asso-ciated with hyperacute ischemic infarction; that is, high signal intensity on diffusion-weighted images and low signal intensity on ADC map. The finding of high signal intensity on T2-weighted images and lesional enhancement on contrast-enhanced T1-weighted images in type 1 lesions

in the present study differ from the findings in ischemic infarction at the same stage. These discrepancies occur at the subacute stage of ischemic infarction because of the breakdown of the blood-brain barrier (Sato et al., 1991). However, in cerebral fat embolism, high signal intensity on T2-weighted images and contrast enhancement of the embo-lized brain substance is observed at the hyperacute stage. This can probably be explained by the early occurrence of the dysfunction of the blood-brain barrier, caused by either the fat itself of the resulting toxicity. To our knowledge, clinical MR imaging findings of hyperacute cerebral fat embolism have not been described previously. A subclinical fat embolism probably occurs after almost all long-bone fractures, but the incidence of the clinically apparent syn-drome is reported to be 0.5~10% in cases of fracture. The full syndrome develops 12 hours to 3 days after injury and is manifested by respiratory distress, encephalopathy, and cutaneous petechiae (Jacobson et al., 1986). The CT and MR imaging findings of clinical cerebral fat embolism syn-drome suggest that the lesions are widespread in the gray matter and white matter in the acute phase and that the lesions are confined primarily to the white matter in the subacute phase (Citerio et al., 1995; Chrysikopoulos et al., 1996; Finlay et al., 1996).

Cerebral fat embolism induced by triolein and oleic acid resulted in both cytotoxic and vasogenic edema, as depicted at MR imaging and electron microscopy. The effects were more severe in the oleic acid group. These findings imply that both triolein and oleic acid damage the blood-brain barrier and that oleic acid is more toxic th the act brain.

REFERENCES

Citerio G, Bianchini E, Beretta L. Magnetic resonance imaging of cerebral fat embolism: a case report. Intensive Care Med. 1995. 21: 679-681.

Chrysikopoulos H, Maniatis V, Pappas J. Case report: posttrau-matic cerebral fat embolism: CT and MR findings-report of two cases and review of the literature. Clin Radiol. 1996. 51: 728-732.

Drew PA, Smith E, Thomas PD. Fat distribution and changes in the blood brain barrier in a rat model of cerebral arterial fat embolism. J Neurol Sci. 1998. 156: 138-143.

Finlay ME, Benson MD. Case report: magnetic resonance imaging in cerebral fat embolism. Clin Radiol. 1996. 51: 445-446.

Jacobson DM, Terrence CF, Reinmuth OM. The neurologic man-
ifestations of fat embolism. Neurology. 1986. 36: 847-851.

Jones JG, Minty BD, Beeley JM, Royston D, Crow J, Grossman
RF. Pulmonary epithelial permeability is immediately increa-
sed after embolisation with oleic acid but not with neutral fat.
Thorax. 1982. 37: 169-174.

Kim HJ, Lee CH, Lee SH, et al. Early development of vasogenic
edema in experimental cerebral fat embolism in cat. Invest
Radiol. 2001. 36: 460-469.

Kroll RA, Neuwelt EA. Outwitting the blood-brain barrier for
therapeutic purposes: osmotic opening and other means-topic
review. Neurosurgery. 1998. 42: 1083-1100.

Moylan JA, Birnbaum M, Katz A, Everson MA. Fat embolism
syndrome. J Trauma. 1976. 16: 341-347.

Nakata Y, Tanaka H, Kuwagata Y, Yoshioka T, Sugimoto H.
Triolein-induced pulmonary embolization and increased mi-
crovascular permeability in isolated perfused rat lungs. J
Trauma. 1999. 47: 111-119.

Peltier LF. Fat embolism: a current concept. Clin Orthop. 1969.
66: 241-253.

Peltier LF, Wheeler DH, Boyd HM, Scott JR. Fat embolism, II;
the chemical composition of fat obtained from human long
bones and sub cutaneous tissue. Surgery. 1956. 40: 661-664.

Cossling HR, Pellegrini VD Jr. Fat embolism syndrome: a review
of the pathophysiology and physiological basis of treatment.
Clin Orthop. 1982. 165: 68-82.

Reidbord HE. Pulmonary fat embolism: and ultrastructural study.
Arch Pathol. 1974. 98: 112-125.

Sato A, Takahashi S, Soma Y, et al. Cerebral infarction: early
detection by means of contrast-enhanced cerebral arteries at
MR imaging. Radiology. 1991. 178: 443-439.